Scaling in a Geothermal Heat Exchanger at Soultz-Sous-Forêts (Upper Rhine Graben, France): A XRD and SEM-EDS Characterization of Sulfide Precipitates

Béatrice A Ledésert, Ronan L Hébert, Justine Mouchot, Clio Bosia, Guillaume Ravier, Olivier Seibel, Éléonore Dalmais, Mariannick Ledésert, Ghislain Trullenque, Xavier Sengelen, et al.

geosciences

MDPI

Article

Scaling in a Geothermal Heat Exchanger at Soultz-Sous-Forêts (Upper Rhine Graben, France): A XRD and SEM-EDS Characterization of Sulfide Precipitates

Béatrice A. Ledésert [1,*], Ronan L. Hébert [1], Justine Mouchot [2], Clio Bosia [2], Guillaume Ravier [2], Olivier Seibel [2], Éléonore Dalmais [2], Mariannick Ledésert [3,†], Ghislain Trullenque [4], Xavier Sengelen [1] and Albert Genter [2]

1 CY Cergy Paris Université, Géosciences et Environnement Cergy, 1 Rue Descartes, 95000 Neuville-sur-Oise, France; ronan.hebert@cyu.fr (R.L.H.); xavier.sengelen@cyu.fr (X.S.)
2 Électricité de Strasbourg Géothermie, 26 Boulevard du Président Wilson, 67000 Strasbourg, France; justine.mouchot@arverne.earth (J.M.); clio.bosia@es.fr (C.B.); guillaume.ravier@es.fr (G.R.); olivier.seibel@es.fr (O.S.); eleonore.dalmais@es.fr (É.D.); albert.genter@es.fr (A.G.)
3 Cristallography Laboratory, 14000 Caen, France; ledesert@cyu.fr
4 UniLaSalle, Collège Géosciences, équipe B2R, 19 Rue Pierre Waguet, 60000 Beauvais, France; ghislain.trullenque@unilasalle.fr
* Correspondence: beatrice.ledesert@cyu.fr; Tel.: +33-134257357
† Retired.

Citation: Ledésert, B.A.; Hébert, R.L.; Mouchot, J.; Bosia, C.; Ravier, G.; Seibel, O.; Dalmais, É.; Ledésert, M.; Trullenque, G.; Sengelen, X.; et al. Scaling in a Geothermal Heat Exchanger at Soultz-Sous-Forêts (Upper Rhine Graben, France): A XRD and SEM-EDS Characterization of Sulfide Precipitates. *Geosciences* **2021**, *11*, 271. https://doi.org/10.3390/geosciences11070271

Academic Editors: Jesus Martinez-Frias and Matteo Alvaro

Received: 5 May 2021
Accepted: 23 June 2021
Published: 28 June 2021

Abstract: The Soultz-Sous-Forêts geothermal site (France) operates three deep wells for electricity production. During operation, scales precipitate within the surface installation as (Ba, Sr) sulfate and (Pb, As, Sb) sulfide types. Scales have an impact on lowering energy production and inducing specific waste management issues. Thus scaling needs to be reduced for which a thorough characterization of the scales has to be performed. The geothermal brine is produced at 160 °C and reinjected at 70 °C during normal operation. In the frame of the H2020 MEET project, a small heat exchanger was tested in order to allow higher energy production, by reinjecting the geothermal fluid at 40 °C. Samples of scales were analyzed by XRD and SEM-EDS, highlighting that mostly galena precipitates and shows various crystal shapes. These shapes can be related to the turbulence of the flow and the speed of crystal growth. Where the flow is turbulent (entrance, water box, exit), crystals grow quickly and mainly show dendritic shape. In the tubes, where the flow is laminar, crystals grow more slowly and some of them are characterized by well-developed faces leading to cubes and derived shapes. The major consequence of the temperature decrease is the increased scaling phenomenon.

Keywords: Soultz-Sous-Forêts; geothermal site; heat exchanger; scales; sulfates; sulfides; As and Sb-bearing galena; crystal growth; crystal shapes

1. Introduction

Geothermal power production is a very attractive resource with characteristics such as low cost, little environmental pollution and worldwide distribution [1–3]. In addition, it is available all the time, whatever climatic conditions and day/night alternation, as opposed to wind- or solar-derived energy. Geothermal power plants take their energy from deep underground water that is pumped to the surface. During its residence time in the ground at sometimes high temperature (150–300 °C), the water acquires specific properties by interaction with the rock reservoir, generally resulting in high salinity and acidity. These characteristics are responsible for corrosion and scaling (deposition) issues in wells and in surface installations. Those phenomena are known from the very beginning of industrial high-temperature geothermal operations and are identified to be responsible for economic issues [4,5]. Scaling is encountered in both low enthalpy [6] and high enthalpy [5,7] geothermal systems. According to [8], among the most abundant scales are silica, carbonates, sulfates, sulfides, and native metals such as antimony (Sb). It is also

known that metal sulfide scaling frequently occurs in volcanic geological context or high Cl environments [9].

Among all the geothermal geological contexts, grabens present specific characteristics. In the Upper Rhine Graben (URG; at the border between France and Germany) hydrothermal fluids percolate within fault zones and are brought relatively close to the surface, favoring the development of high-energy geothermal plants. These are dedicated to the production of either electricity (e.g., Soultz-Sous-Forêts, called Soultz in the following) or heat (e.g., Rittershoffen). The URG deep ground water system is characterized by a brine with high salinity (99–107 g/L at Soultz) and moderate low pH (around 5) [10] responsible for strong corrosion of geothermal surface installations (pipes, heat exchangers) and also deposition of minerals within these installations [11,12].

The Soultz geothermal production plant is based on three 5000 m-deep wells, GPK-2, GPK-3 and GPK-4 (Figure 1) penetrating the granitic basement. GPK-2 is the production well while the total reinjection of the geothermal fluid is performed through GPK-3 and GPK-4. In industrial operation conditions, the brine is produced at 160 °C and is reinjected at 70 °C [13], showing no difference in its chemical composition when the temperature decreases. In the framework of the H2020 MEET European program [14,15], an additional small heat exchanger (SHEx) has been installed temporarily in order to assess the optimization of energy production by lowering the temperature of the reinjected fluid from 70 °C to 40 °C [16]. This SHEx received 10% of the total flow and was tested over 3 months. It was designed with six alloys in order to test their reaction to corrosion and scaling. Only scaling phenomena are described here and several points are addressed: (1) determination of the chemical and mineralogical composition of the scales, (2) impact of temperature lowering on the scaling processes (composition/morphology/thickening of the deposits), (3) influence of alloys on scaling development. An X-ray diffraction (XRD) and scanning electron microscopy coupled with energy dispersive spectrometry (SEM-EDS) survey was performed to answer those questions.

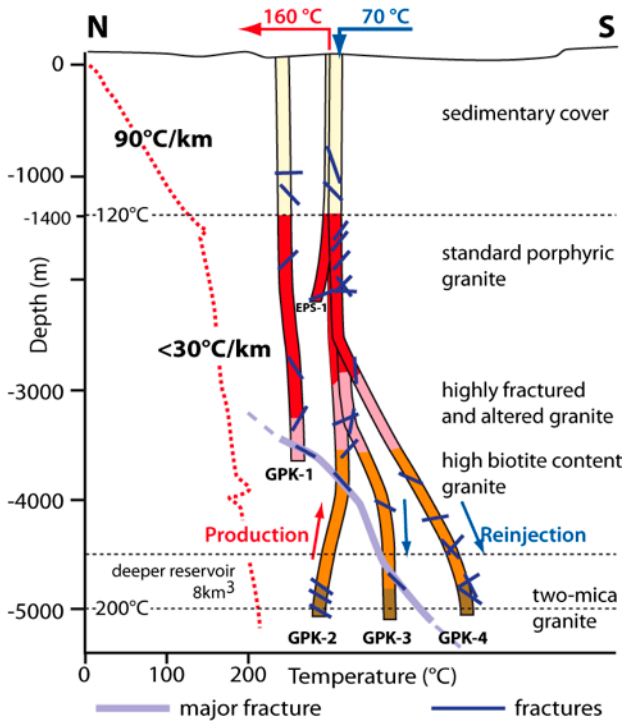

Figure 1. The Soultz Enhanced Geothermal System with its 5 wells among which the 3 deepest ones (GPK-2, GPK-3 and GPK-4) are used for electricity production. The brine is produced at 160 °C in GPK-2 well and reinjected at 70 °C in GPK-3 and GPK-4 in normal operation. The temperature gradient recorded at Soultz (red dashed line) and key figures are indicated on the left. Figure modified after [17,18]; size of the deep reservoir from [19].

2. Technical Context

2.1. Scaling Phenomenon in Geothermal Power Plants Worldwide

Scaling is a common phenomenon in geothermal power plants worldwide. Specific site analyses on scaling issues occurring in various geothermal plant types are reported in abundant literature [12,20–30], showing the importance of this topic for the plant operation. Scales act as insulators and thus lower the thermal exchanges. They also reduce the diameter of the pipes and inside volume of the exchangers which lowers the overall productivity of the geothermal power plants. Scales may also trigger the accumulation of toxic chemical elements, inducing additional risk and cost issues during the operational phase. In addition, scale formation is generally linked to degassing process, which has a major impact in terms of corrosion on the surface installation of geothermal power plants. Reducing the formation of scales is a challenge for operators who thus use inhibitors in their industrial process in order to prevent their formation [2,21,31].

2.2. Scaling Phenomeon at Soultz Geothermal Power Plant

At Soultz, surface installations are composed of several parts among which pipes and heat exchangers in which the natural geothermal fluid provides its thermal energy to an industrial fluid. An Organic Rankine Cycle (ORC) allows the production of electricity. The temperature of the brine lowers within the exchangers and the chemical equilibrium changes, resulting in the precipitation of minerals. The geochemistry of the brine provided by [10,13] shows a high salinity due to a great abundance of Na, K and Ca as major cations and Cl and SO_4 as major anions. It is summarized in Table 1, for the elements found in the scales. Li, Zn, Ba and other minor elements are also present in significant abundance. In addition, the geothermal fluid is characterized by a high CO_2 content, and natural anoxic conditions [10,13].

Table 1. Chemical composition of the brine after [10,13] from 22 brine samples collected in GPK-1, and the three deep wells at Soultz. Sb is not given in [13] (ng: not given), the only data about Sb comes from [10]. MRCC: most representative chemical composition of the native geothermal brine, in [13].

	Na (g/L)	K (g/L)	Ca (g/L)	Mg (mg/L)	Cl (g/L)	SO_4 (mg/L)	SiO_2 (mg/L)	As (mg/L)	Sb (µg/L) in [10]	Pb (µg/L)
Min-max values [13]	21–28.2	2.38–3.38	3.46–7.30	75–411	32.6–61	150–255	63–409	0.6–11	ng	181–782
MRCC [13] except for Sb	27.5	3.25	6.90	125	59	159	427	6	57.4	300

From this brine, sulfates of barite type ((Sr, Ba)SO_4) and minor sulfides of galena type ((Pb, As, Sb)S) precipitate during the lowering of the temperature in surface installations when no antiscalants are used [27,30]. The same phenomenon is also encountered in German geothermal plants located in the URG [12]. In the URG, and at Soultz in particular where the geothermal brine circulates within a granitic basement, those scales are known to accumulate radionuclides, ^{226}Ra for sulfates and ^{210}Pb for sulfides [30], and are thus to be disposed of as Naturally Occurring Radioactive Material waste (NORM classification, [32]. In such conditions when no inhibitors were used, the Soultz power plant needed to be stopped and cleaned three times a year, inducing high maintenance cost, loss of energy production and waste management issues [33].

For safety reasons and power plant healthy operation, the formation of barite needs to be inhibited continuously [31,33]. Antiscalants are well known from the oil and gas industry and mainly consist of phosphonates and polycarboxylates when preventing barite formation [34]. The scaling phenomenon being closely linked with corrosion phenomena described by [35–37], both an antiscalant and a corrosion inhibitor are currently used at Soultz. The corrosion inhibitor agent is based on amines. Each type of mineral scale has an antiscalant which is more suitable for lowering its deposited amount. Antiscalants are

either inhibitors of crystallization known to be very powerful to control barite deposition or dispersants that better control metal sulfide scaling [33], or even a mixture of both. When sulfate production is made impossible thanks to antiscalants, sulfides precipitate as observed by [12] in geothermal power plants of the URG. In the following, chemicals used to prevent the deposition of scales will be simply called inhibitors.

2.3. The Tested Small Heat Exchanger (SHEx; Soultz)

In a geothermal exchanger, the natural hot brine provides its thermal energy to a working fluid and then is reinjected. Both flows are totally independent of one another and never mix. The SHEx was installed as bypass on the reinjection line [17]. It was tested over three months (late January to April 2019) in the presence of inhibitors, after which it was dismantled to allow scaling and corrosion studies. The SHEx consists of a tubular heat exchanger made with tubes of six different alloys (Figure 2), an entrance, an exit, and one water box at each end with different designs (Figure 2A) made of a seventh alloy. The west water box is separated into three compartments, while the east one is made of only two parts (Figure 2B). The cross-section of the shirt and the included tubes with their alloy is shown in Figure 2C. The tubes are organized in three parallel layers. The hot fluid comes into the SHEx through the entrance and flows through the three layers of tube with a constant decrease of the temperature: around 65–70 °C at the entrance, ~60 °C in the upper layer of tubes, 50 °C in the intermediate layer, then 40 °C in the lower layer and the exit (Figure 2B). Each water box is closed by a flange (Figure 2D).

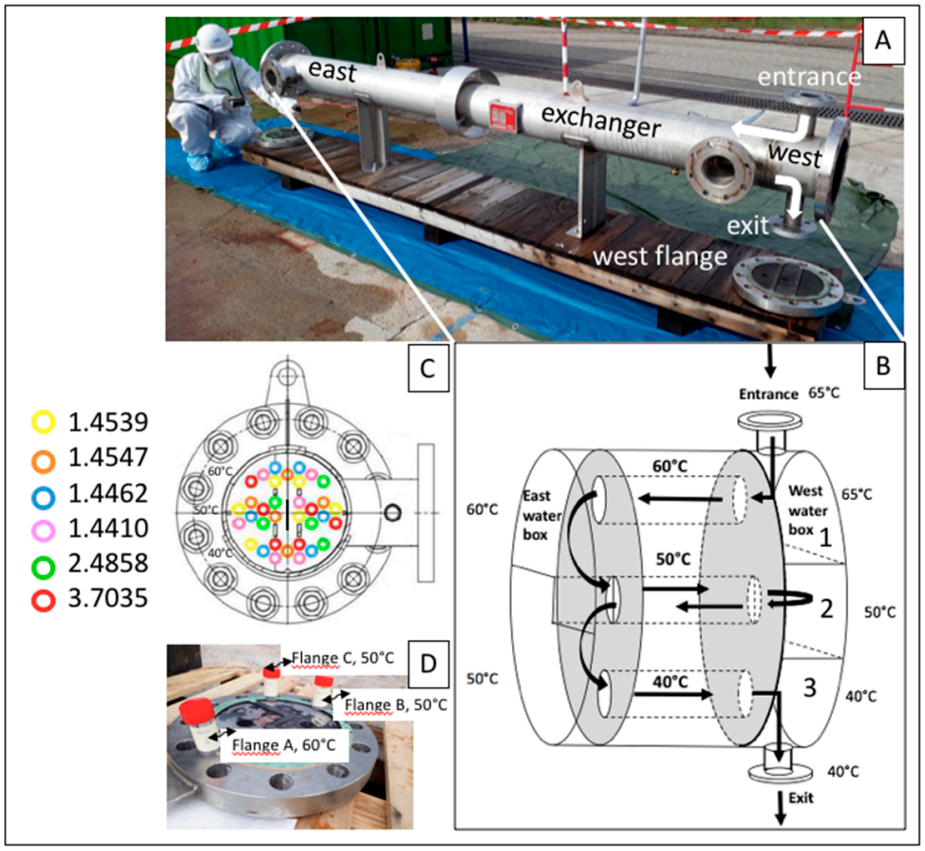

Figure 2. (**A**) overview of the SHEx; (**B**) schematic section of the cooling-down loop with 4 passes; (**C**): schematic front view with the tested alloys after [17]; (**D**): location of samples on flange closing the east water box. Note that only one tube is represented in (**B**) for each temperature (see Figure 2C for exact front representation of the location of tubes, after [17]). The intermediate layer of tubes is separated vertically in two parts (Figures 2B,C and 3) as can be seen in the east water box. Only the circulation of the geothermal brine is schematized.

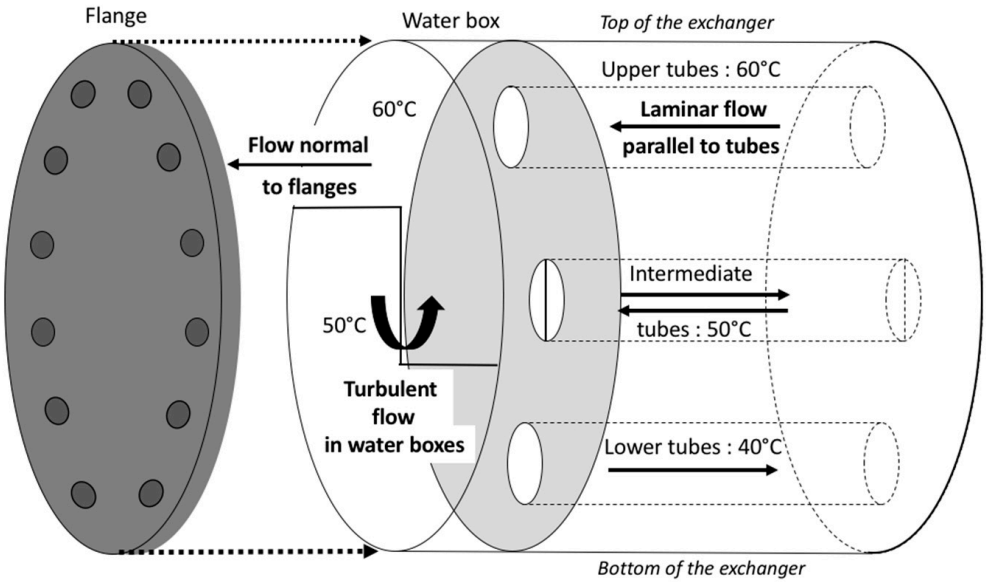

Figure 3. Temperature and flow inside the exchanger. Note that only one tube is represented for each temperature (see Figure 2C for exact cross section representation of the location and alloy of tubes). The intermediate layer of tubes is separated in two parts by a vertical panel. Thus, the flow occurs in both directions but in separate tubes. The west water box is not represented.

The path followed by the geothermal fluid within the SHEx and the flow regime is shown in Figure 3: turbulent in the entrance and in water boxes, laminar into the tubes, and perpendicular to the flanges, hence allowing to examine the likely influence of the flow regime on the scales. The three layers of tubes allow the examination of the likely impact of temperature on the scaling phenomenon. The six tested alloys are 1.4539 (904 L), 1.4547 (254 SMO), 1.4462 (DX 2205), 1.4410 (SDX 2507), 2.4858 (Alloy 825) and 3.7035 (TiGr2) [17] as visible in Figure 2C. The potential influence of the alloys on the scales will also be discussed. Mundhenk (2012) [26] proposed a ranking of metals as regards corrosion in geothermal brine conditions of the URG. The industrial exchangers currently operated at Soultz and Rittershoffen are made of 1.4410 (SDX 2507).

3. Material and Methods

3.1. Scales

In this fluid circulation test performed with the use of inhibitors, scales occur as black deposits, either as a powder (for example in water boxes, Table 2), or as a continuous plating forming a thin solid layer (like in tubes, Figure 4).

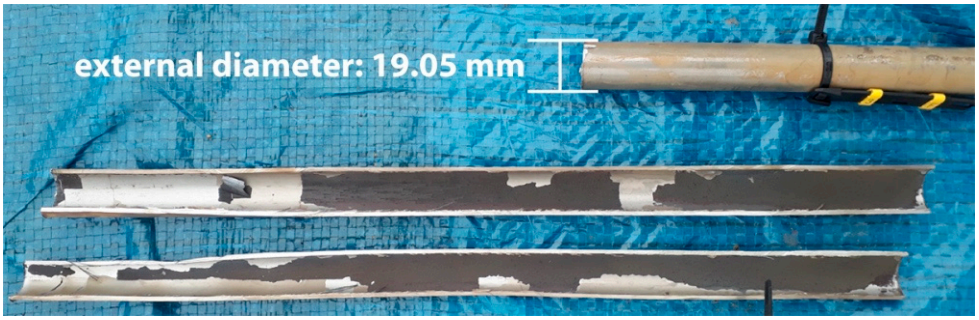

Figure 4. Macroscopic view of continuous scales while still in contact with a metal tube during dismantling of the SHEx in April 2019. The tube has been cut all along for the recovery of scales.

3.2. Preparation of Samples

The SHEx was only drained and not rinsed before dismantling. Thirty-five samples were collected in the SHEx and one in the operated industrial plant for SEM-EDS analyses (Table 2). They were collected in order to be representative of hydrodynamic and thermal conditions for each alloy. They were neither rinsed with clear water nor ground. They were simply dried at ambient temperature. The industrial sample was collected in 2017 in the operated power plant at the exit of the industrial heat exchanger, just before the reinjection line, where the geothermal fluid is circulating at a temperature of 75–65 °C in contact with a 1.4410 steel.

Millimeter-size fragments of continuous solid scales were collected and glued on metal stubs with carbon lacquer (Figure 5) for observation by reflection optical microscopy (ROM) and scanning electron microscopy (SEM) coupled with energy dispersive spectrometry (EDS) for local chemical analyses. For each sample, the side in contact with the metal (called metal side, MS in the following), the side in contact with the fluid (called fluid side, FS in the following) and the cross-section were prepared systematically (Figure 5). The MS surface looks bright and smooth while FS surface is velvety and rough (Figures 4 and 5). The cross-section was prepared in order to study the thickness of the deposits, but the preparation frequently failed. It is to be noted that on alloy 1.4462, the scales separated systematically into two layers (MS and FS) during sampling, which is the reason why three samples were collected for each temperature (MS, FS and total). Scales from industrial sample, entrance and water boxes of the SHEx occur as a powder (Figure 6) and they were just spread over carbon lacquer (Figure 6).

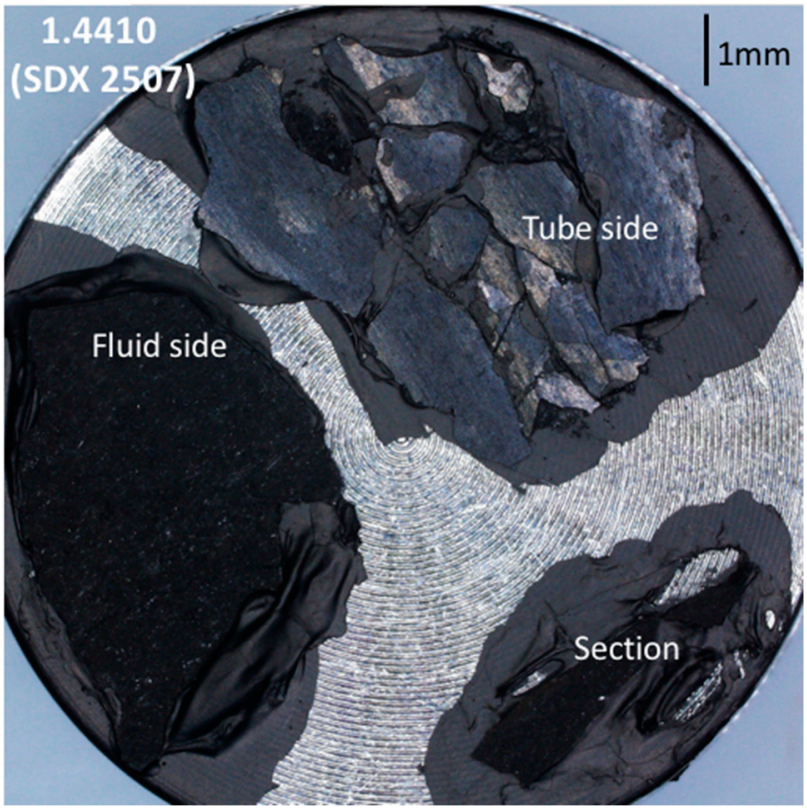

Figure 5. ROM view of tiny samples of continuous scales with smooth MS (tube side), velvety rough FS and section of samples collected in a tube made of 1.4410 super duplex steel, at 60 °C, glued with carbon lacquer on a metal stub for SEM-EDS analysis.

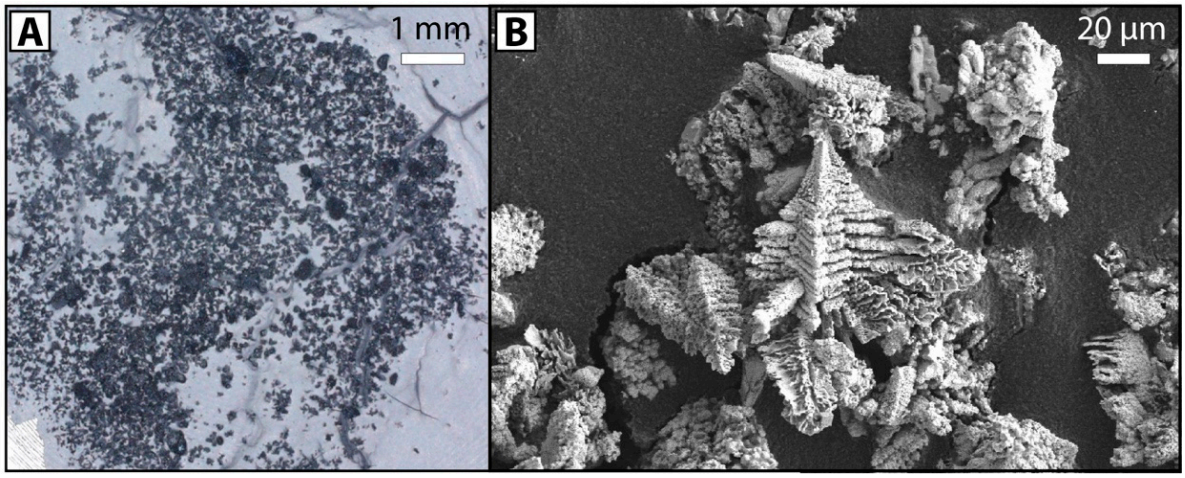

Figure 6. Powder collected in the entrance of the SHEX made of 1.4307, (**A**) as viewed by ROM and (**B**) by SEM.

3.3. X-ray Diffraction

More than 1 g of scales being necessary for X-ray diffraction (XRD), the amount of scales was insufficient in any tube of the SHEx. Only entrance, exit and water boxes 1 and 3, all of them made of 1.4307, provided 4 samples. XRD was performed by ORANO company with a Panalytical diffractometer using Co Kα radiation (λ = 1791 Å) in order to avoid potential Fe fluorescence. Neither internal nor external standards were used. The results were compared to JCPDS files for the determination of the mineral phases present in the samples.

3.4. Scanning Electron Microscopy Coupled with Energy Dispersive Spectrometry (SEM-EDS)

The SEM used in this study, a Zeiss GeminiSEM 300 coupled with a Bruker EDS, belongs to the IMAT analysis facility of CY Cergy Paris Université. No metal coating was necessary prior to observation. Observation was performed with a secondary electron detector by using a chosen acceleration voltage (between 10 and 15 kV) at a working distance between 6 and 8 mm that allowed EDS analyses in high vacuum mode. A low acceleration voltage was deliberately chosen in order to lower the beam/sample interaction volume size and to ascertain that the X-ray pulses came exclusively from the scale particles. This modest acceleration voltage presents a second advantage as it reduces significantly charging phenomena. However, this induces a poor quality of analyses enhanced by the marked topography of samples which is not ideal in terms of quantification as the beam/sample interaction volume might be truncated or shadowed. Thus, the analyses can only be used for relative abundance of the elements within and between the different scale samples.

4. Results

Results obtained by XRD and SEM-EDS are presented below and discussed in Section 5.

4.1. X-ray Diffraction (XRD)

XRD patterns that were obtained for the four samples are provided in Figure 7. Entrance and exit of the SHEx show the same diffractograms, indicating the presence of galena (PbS), and likely minor dufrénoysite ($Pb_2As_2S_5$) as regards the weak intensity of the peaks, over the whole range of temperatures (65 °C and 40 °C). The water boxes also show the presence of galena and likely dufrénoysite, together with that of halite (NaCl) for the two temperatures under concern (65 °C and 40 °C). The samples not being reduced into powder it was possible to determine hkl diffraction planes for galena, namely 111, 200, 220, 311 and 222 (Figure 7).

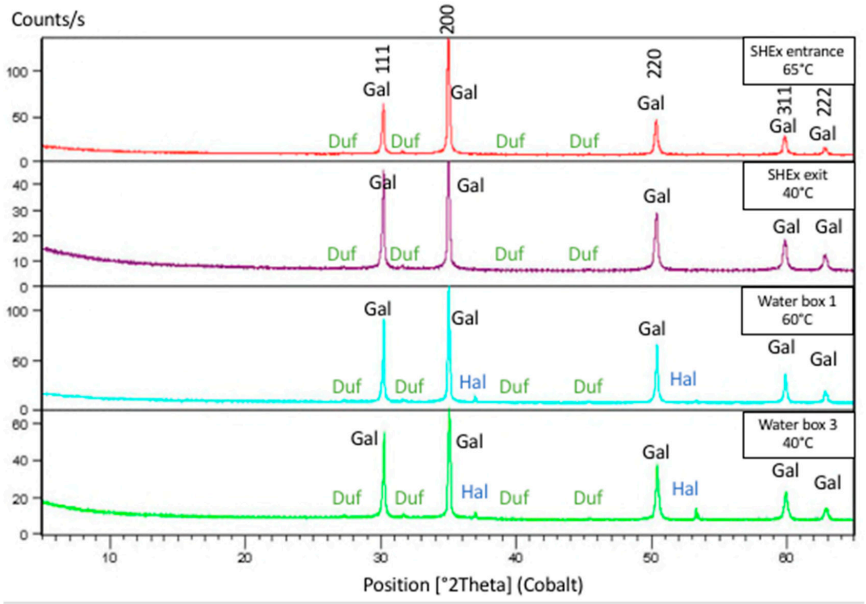

Figure 7. X-ray diffraction diagrams obtained for scales collected in the entrance, the exit and water boxes 1 and 3 of the SHEx. They show galena (Gal; As and Sb bearing PbS), additional halite (Hal; NaCl) in the water boxes, and likely traces of dufrénoysite (Duf; Pb2As2S5), all of these sites being made of 1.4307 alloy. The numbers indicated vertically represent the hkl diffraction planes of galena crystals.

4.2. Scanning Electron Microscopy coupled with Energy Dispersive Spectrometry (SEM-EDS)

The observation by SEM allows to distinguish several features.

4.2.1. Structure of the Scales

As indicated before, scales occur as a continuous solid deposit (Figure 5) or as a powder (Figure 6, Table 2). In that first case, the deposit shows a rough FS in contact with the geothermal brine (Figure 8A,B) and a smooth MS in contact with the metal (Figure 8C,D).

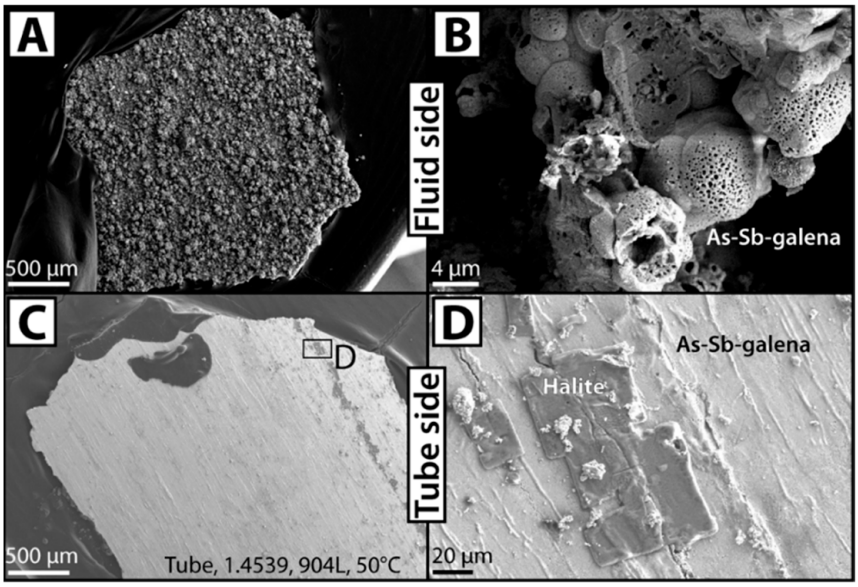

Figure 8. Sample 1.4539, 50 °C, surface of the scales: rough in contact with the brine (**A** and zoom in **B**), smooth in contact with the metal (**C** and zoom in **D**), showing As-Sb-galena and halite on MS and only galena on FS in this example.

Table 2. Summary of sampling points, performed analyses and observation by SEM. Industrial: industrial heat exchanger. All other sampling points are within the SHEx. FS: fluid side, MS: metal side, Total: FS+MS sampled at the same time when they separate. The alloys are from [17]. The analyses performed on each sample are indicated. Wwb: West water box. (co): cuboctahedron. (oct): octahedron. Underlined figures are for 1.4410 alloy for comparison between three temperatures.

Sampling Points	Alloy	Temperature (°C)	Structure of scales	Analyses	Whole Thickness of Scales (µm)	Thickness of Smooth Zone (µm)	Dendrite	Needle	Coral	Cube	Fibro-Radiated
Industrial	1.4410	65–75	Powder	SEM			x				
Entrance	1.4307	65	Powder	XRD, SEM			x				
Exit	1.4307	40	Powder	XRD							
Wwb 1 (top)	1.4307	65	Powder	XRD, SEM			x	x		x	x
Wwb 2 (Middle)	1.4307	55	Powder	SEM					x		
Wwb 3 (Bottom)	1.4307	40	Powder	XRD, SEM					x		x
Flange A (East)	1.4307	60	Continuous	SEM	-	15	x		x		x
Flange B (East)	1.4307	50	Continuous	SEM	30	12		x	x	x	
Flange C (East)	1.4307	50	Continuous	SEM	110	15					
Tube	1.4539	60	Continuous	SEM				x	x	x (co)	
Tube	1.4547	60	Continuous	SEM					x		
Tube (FS)	1.4462	60	Continuous	SEM					-		
Tube (MS)	1.4462	60	Continuous	SEM					-		
Tube (Total)	1.4462	60	Continuous	SEM	22	5			x?		
Tube	1.4410	60	Continuous	SEM	<u>50</u>	<u>10</u>			x		
Tube	2.4858	60	Continuous	SEM					x		
Tube	3.7035	60	Continuous	SEM	15	6			-		
Tube	1.4539	50	Continuous	SEM				x	x		x
Tube	1.4547	50	Continuous	SEM	270	-			x		x
Tube (FS)	1.4462	50	Continuous	SEM					-		
Tube (MS)	1.4462	50	Continuous	SEM					-		
Tube (Total)	1.4462	50	Continuous	SEM					x?		
Tube	1.4410	50	Continuous	SEM	<u>80</u>	<u>10</u>			x		x
Tube	2.4858	50	Continuous	SEM	50	30		x	x		x
Tube	3.7035	50	Continuous	SEM					x		
Tube	1.4539	40	Continuous	SEM	200	10			x		
Tube	1.4547	40	Continuous	SEM	270	25			x		
Tube (FS)	1.4462	40	Continuous	SEM							
Tube (MS)	1.4462	40	Continuous	SEM							
Tube (Total)	1.4462	40	Continuous	SEM				x	x	x (oct)	x
Tube	1.4410	40	Continuous	SEM	<u>220</u>	<u>10</u>			x		
Tube	2.4858	40	Continuous	SEM	60	30			x		x
Tube	3.7035	40	Continuous	SEM							

The scales are composed of several superimposed layers (Figure 9A) and the smooth layer in contact with the metal is generally divided in several parallel sub-layers (Figure 9B).

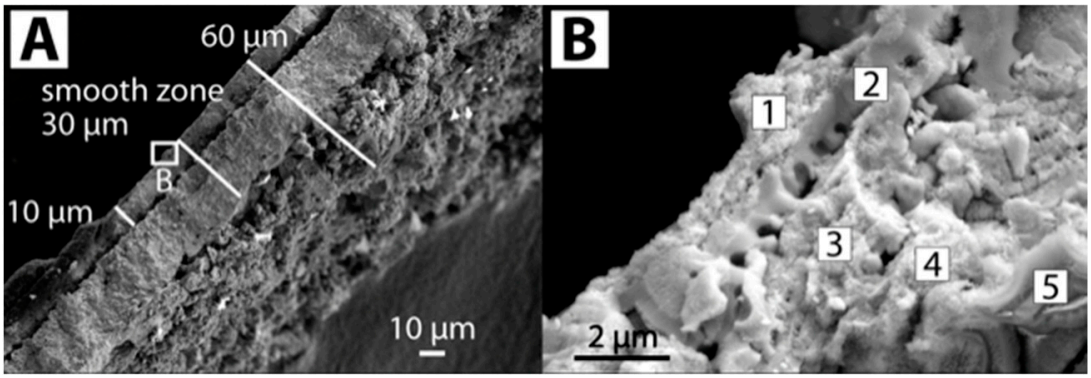

Figure 9. Sample of scales collected in a tube made of 2.4858 at 40 °C. (**A**) Cross-section of the scales divided into several layers, (**B**) the very first one (in contact with the metal) being itself composed of several micro-porous sub-layers. B is a focus on the white rectangle in A and shows five successive sub-layers that deposited on the top of one another. Sub-layer 1 is the oldest, in direct contact with the metal.

4.2.2. Thickness of the Scales

The thickness of scales was measured whenever it was possible, which was not very frequent. It could be measured systematically only for scales deposited in tubes made of 1.4410 (Figure 10) at decreasing temperatures. One has to note that measuring the thickness by SEM provides values with a non-negligible uncertainty as the measurement was sometimes not exactly normal to the deposit. However, the magnitude of the measurement remains true. The thickness observed in tubes of 1.4410 after the 3-month test was around 50 µm at 60 °C, 80 µm at 50 °C and locally up to 220 µm at 40 °C (Table 2, Figure 10), thus representing a deposition rate of about 17 µm/month at 60 °C to 73 µm/month at 40 °C, considering a constant deposition rate. The same trend of increasing thickness with decreasing temperatures tends to be seen on other alloys (Table 2): small at 60 °C (22, 50, and 15 µm, in tubes made of 1.4462, 1.4410, 3.7035 respectively), generally greater at 50 °C (270, 80, and 50µm, in tubes made of 1.4547, 1.4410, 2.4858 respectively) and in general the biggest at 40 °C (200, 270, 220, 60 µm, in tubes made of 1.4539, 1.4547, 1.4410, 2.4858 respectively).

Wherever it could be measured, the smooth zone always shows a thickness smaller than or equal to 30 µm, while the whole thickness of the deposit reaches 270 µm. Nothing much can be said about the thickness of scales deposited on the east flange as it could not be measured as a whole at 60 °C and varies from 30 to 110 µm at 50 °C. No sample is available at 40 °C as the flange is separated in only two zones: 60 °C and 50 °C.

4.2.3. SEM-EDS Chemistry of the Samples

Whatever the location (water box, entrance, exit and tubes), either on MS or FS of the scales when they are continuous, or in powder, and whatever the alloy on which they deposited, SEM-EDS spectra and maps show the presence of Pb, S ± As and Sb compounds of galena type (Figures 11 and 12). Halite (NaCl) is also frequently observed. Both of these two phases were encountered on the XRD patterns (Figure 7). Because of the analytical limitations exposed in the Methods section and their likely small size, crystals of sulfosalts such as dufrénoysite were not identified by SEM-EDS.

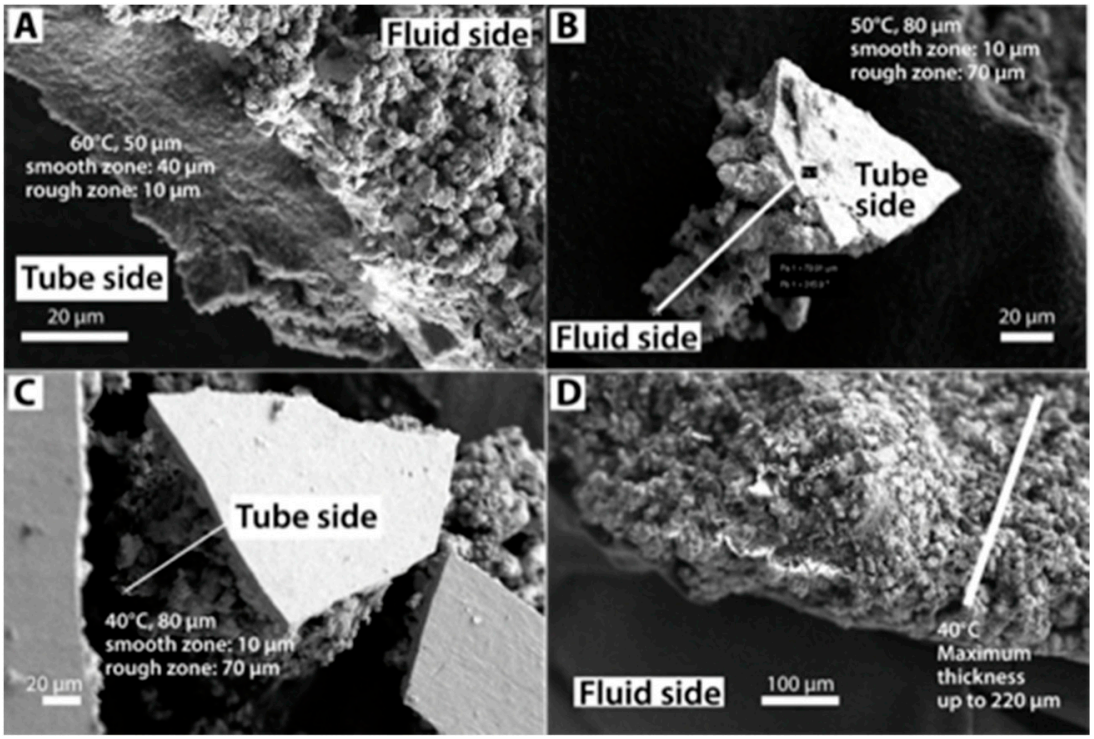

Figure 10. Tubes made of 1.4410, thickness as a function of temperature. The deposit in contact with the metal is smooth while it is rough when in contact with the brine. The thickness of the scales tends to increase when the temperature decreases within the SHEx, from 50 µm at 60 °C to 220 µm at 40 °C. (**A**) 60 °C, (**B**) 50 °C, (**C**,**D**) 40 °C.

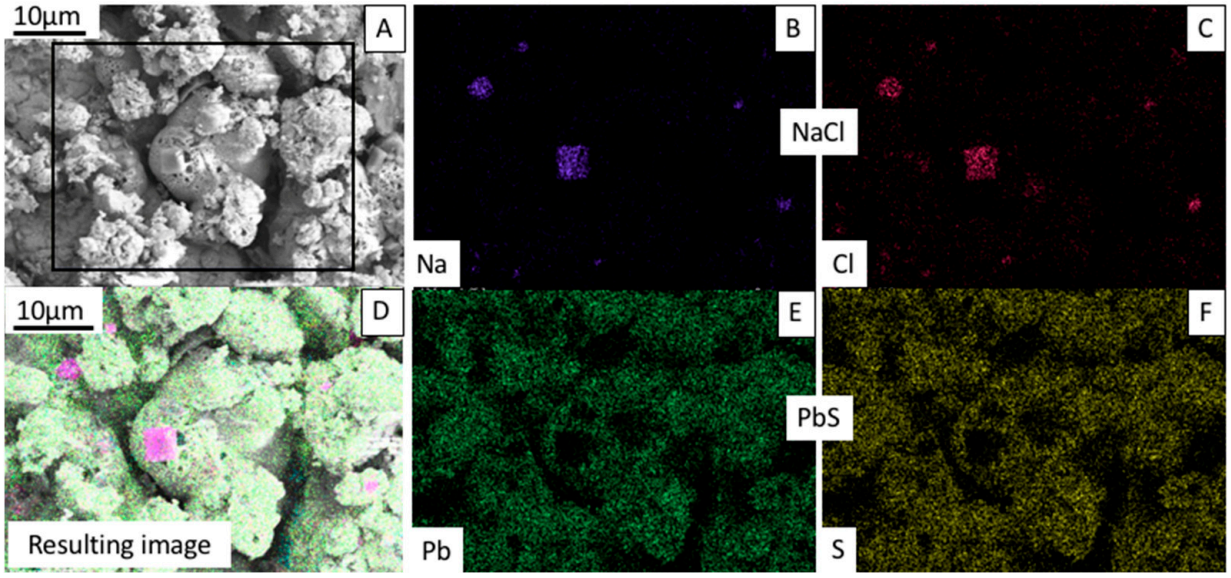

Figure 11. EDS map of FS of scales collected in a tube made of 2.4858, at 40 °C (**A**–**F**) showing (**A**) the SEM image and the black rectangle in which the elementary maps were performed, (**B**,**C**) maps of elementary concentration for Na and Cl characteristic of halite (NaCl) with its common cubic shape, (**D**) resulting map with all elements, (**E**,**F**) maps of elementary concentration for Pb and S characteristic of galena (PbS). As and Sb were also encountered together with Pb and S but in such a small amount that the images are not contrasted enough to be included.

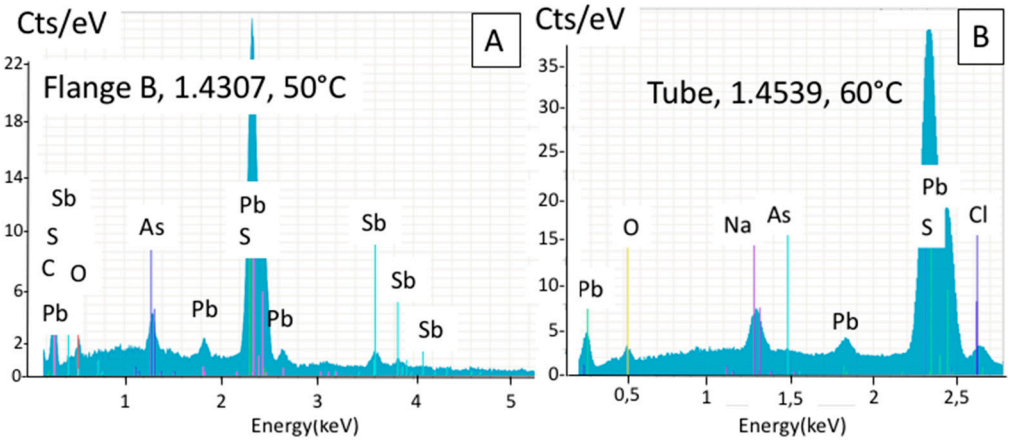

Figure 12. EDS spectra obtained on FS of scales collected (**A**) on a flange at 50 °C and (**B**) in a tube made of 1.4539, at 60 °C.

Table 3 shows examples of semi-quantitative analyses. The same elements (Pb, As, Sb, S) are present in each of the studied samples (analyses 1, 2 and 3), but in varying relative abundance. Sb is sometimes quite abundant (analyses 2 and 3) but no Sb-bearing sulfosalts were discovered either on XRD diagrams (Figure 7) or by SEM. Na and Cl are also locally detected in the samples.

Table 3. Three normalized semi-quantitative analyses obtained by SEM-EDS. Note the limitations of accuracy due to the low acceleration voltage, the topography of samples and their low thickness. The analyses can only be used for relative abundance of the elements within and between the different scale samples and mostly indicate the elements present in the samples.

	1	**2**	**3**
	Tube 3.7035 60 °C	Tube 2.4855 60 °C	Tube 2.4855 40 °C
Elements	Content (wt.%)	Content (wt.%)	Content (wt.%)
S	11.75	16.28	15.00
As	3.89	8.57	3.70
Sb	11.46	25.08	17.82
Pb	72.90	50.07	63.48
Total	100	100	100

From these semi-quantitative results, no difference appears in the chemistry of the scales, whatever the alloy on which they deposited or the temperature of the brine from which they precipitated.

4.2.4. Shapes of Galena Crystals

Various galena crystal shapes were observed thanks to SEM on the tiny fragments described in Section 3 (Materials and Methods). The crystals are of micrometer size in millimeter-sized samples. Thus, these observations might not be exhaustive but give an overview of the crystal shapes of galena.

1. Dendrites

Dendritic crystal shape was observed in the scales collected in the industrial installation (reference sample), as well as in the entrance of the SHEx, and on the upper part of the eastern flange (Figure 13). The industrial sample and that collected at the entrance of the SHEx are made of only dendrites (Figure 13A,B). The only dendrite observed on the flange (Figure 13C) seems to have been deposited by the flow as it is free and not embedded in the matrix. No dendrites were found in any of the tubes, whatever the temperature.

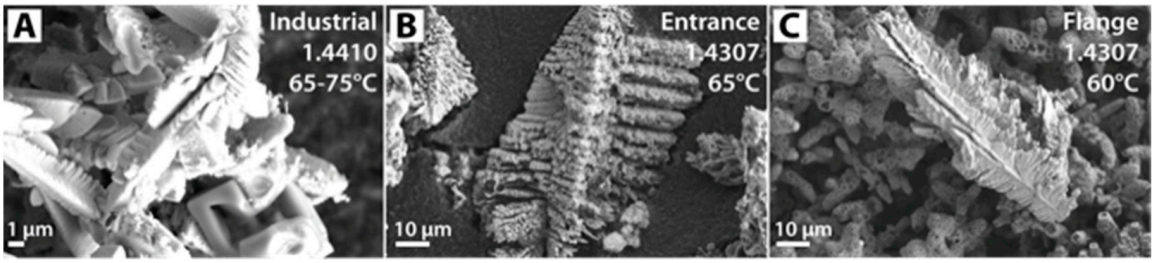

Figure 13. Dendritic shapes of galena crystals (**A**) in the industrial sample (1.4410 alloy), (**B**) in the entrance of the SHEx and (**C**) on the upper part of the eastern flange (both made of 1.4307). No dendrites were found in any of the tubes.

2. Needles

Needle shape is found in tubes of 1.4462 (50 °C and 40 °C), 1.4539 (60 °C and 50 °C), and 2.4858 (50 °C), in water boxes (1.4307 alloy, at 65 °C, 55 °C and 40 °C), and on a flange (1.4307 alloy, 50 °C), thus at various temperatures (from 65 °C to 40 °C, Figure 14) and alloys. Needles were not observed on other samples. Needles can be parallel to each other (A) or perpendicular (B to H) and sometimes in three orthogonal directions (C). Needles have a square section as visible mostly in B and F. They were observed in zones where the flow is rather laminar (tubes) or turbulent (water boxes and flanges).

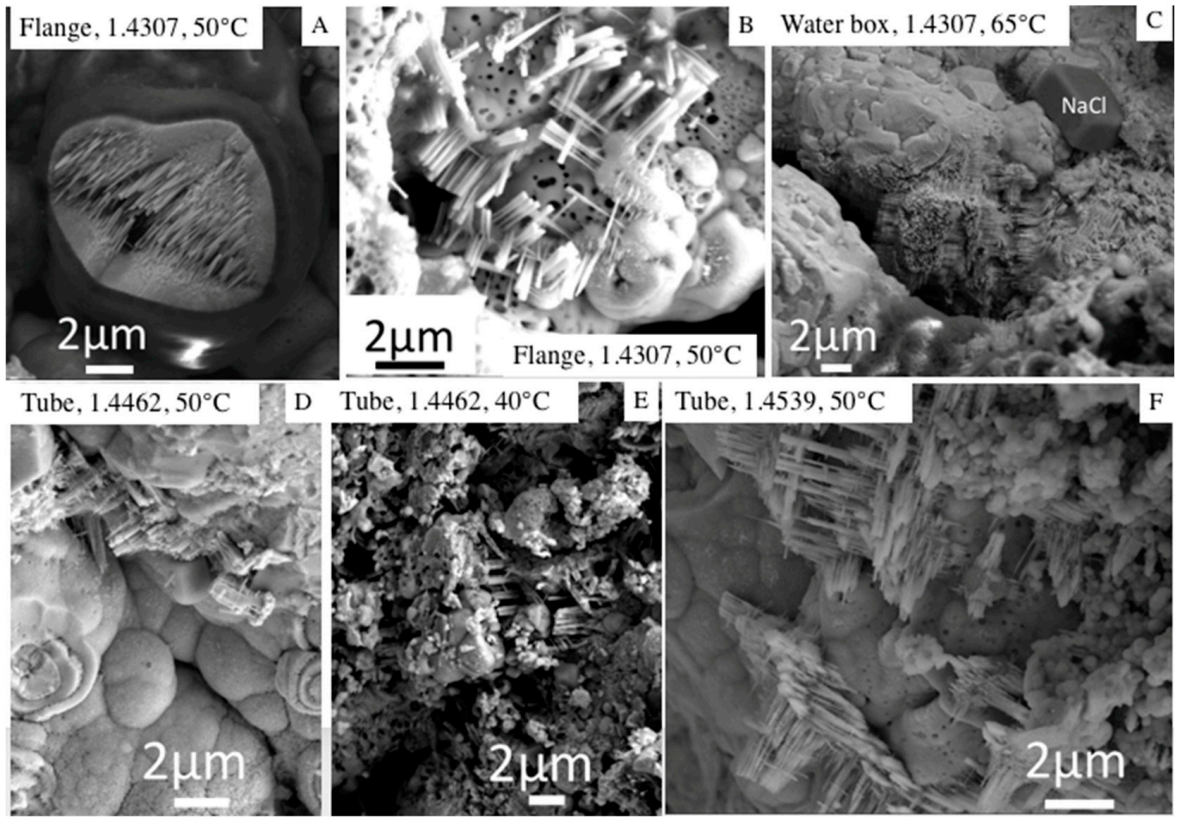

Figure 14. Needle shapes of galena crystals (**A**,**B**) on a flange and (**C**) in water box and (**D**–**F**) in tubes, at different temperatures and on three different alloys (1.4307, 1.4462, 1.4539). (**A**) needles parallel to each other, (**B**–**F**): needles grew in perpendicular directions. (**B**,**F**): Note that the needles are monocrystals with square section.

3. Coral Shapes

Coral-like shapes are of various types (Figure 15) that all show an important internal porosity. They are the most common shapes encountered in the exchanger (Table 4). They were observed in different zones of the SHEx (entrance, 1.4307 alloy; water box, 1.4307

alloy; flange, 1.4307 alloy) and in tubes of all alloys, and at temperatures varying from 65 °C (entrance and water box) to 40 °C (water box and tubes).

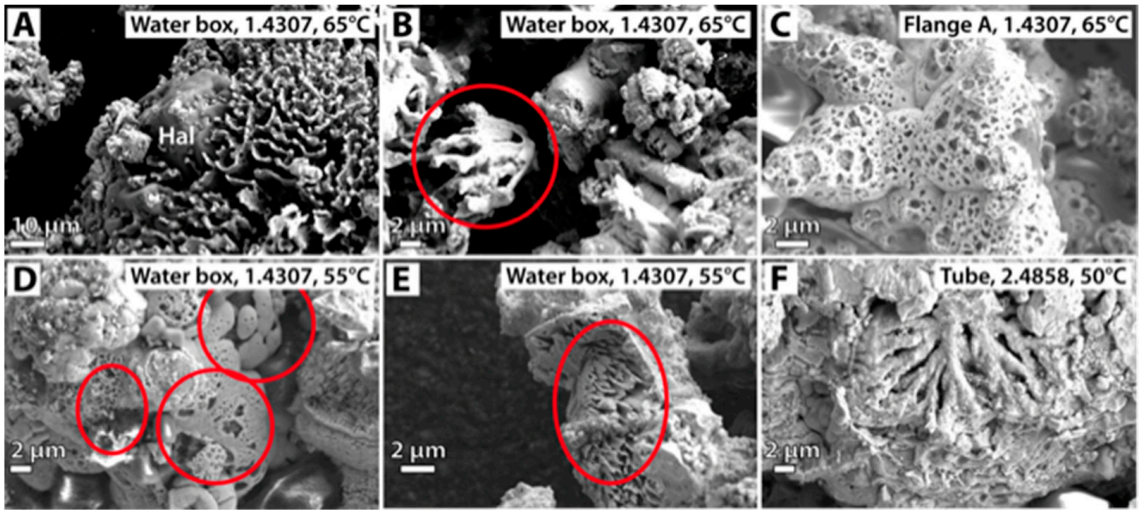

Figure 15. PbS coral shapes of different kinds. All of them show an important internal porosity. The zones to be observed are highlighted by red ellipses. Hal: halite. (**A**) halite crystal embedded in coral shape galena, water box, 1.4307, 65 °C, (**B**) 3D view of coral shape galena, water box, 1.4307, 65 °C, (**C**) coral shape made of botryoids with abundant porosity, flange A, 1.4307, 65 °C, (**D**) coral shape made of botryoids with abundant porosity, water box, 1.4307, 55 °C, (**E**) coral shape made of numerous contiguous needles, water box, 1.4307, 55 °C, (**F**) cross section of coral shape galena.

4. Cube and Cubic-Derived Shapes

Several cubic or cubic-derived shapes were observed in the samples. Cubes were found in a tube at 60 °C (1.4539) where it shows exactly the same hollow shape as on a flange (1.4307, 40 °C; Figure 16A). Cubes were also observed in a water box (1.4307, 40 °C; Figure 16B,C) where they occur either as massive structures (Figure 16B) or as a kind of skeleton made of needles oriented in the three directions of space (Figure 16C), those two features being in close contact in the same sample. Cubes are thus found on at least two different alloys (1.4307 and 1.4539) and at temperatures from 60 °C to 40 °C.

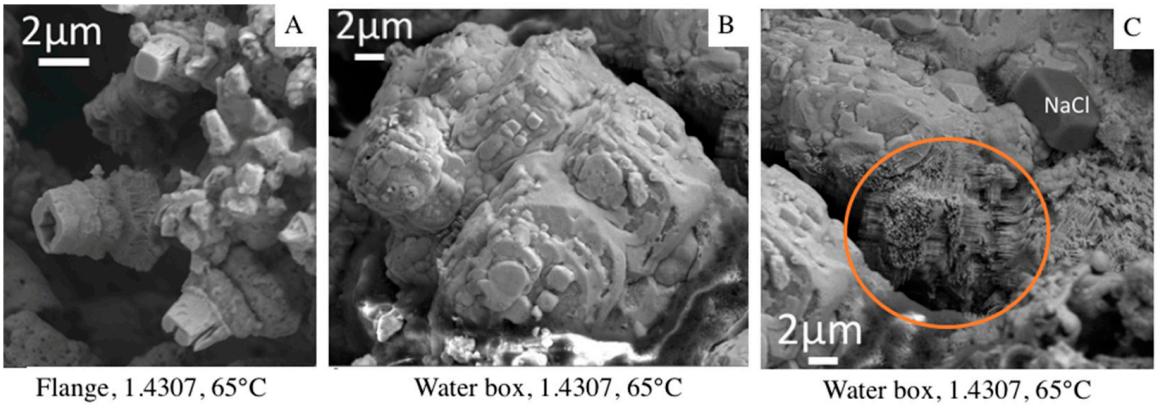

Figure 16. Cubic-derived shape of PbS crystals, occurring as (**A**) hollow cubes, (**B**) massive cubes, or (**C**) skeleton made of needles in three orthogonal directions inside the orange ellipse. The massive cube (**B**) is seen in the lower left-hand corner of (**C**).

Other PbS shapes derived from the cube were locally observed in tubes, as shown in Figure 17, such as a cuboctahedron (Figure 17A) and an octahedron (Figure 17B), on two different alloys and at 60 °C and 40 °C respectively. The octahedron (Figure 17B) in found in the vicinity of orthogonal needles not visible on the photograph.

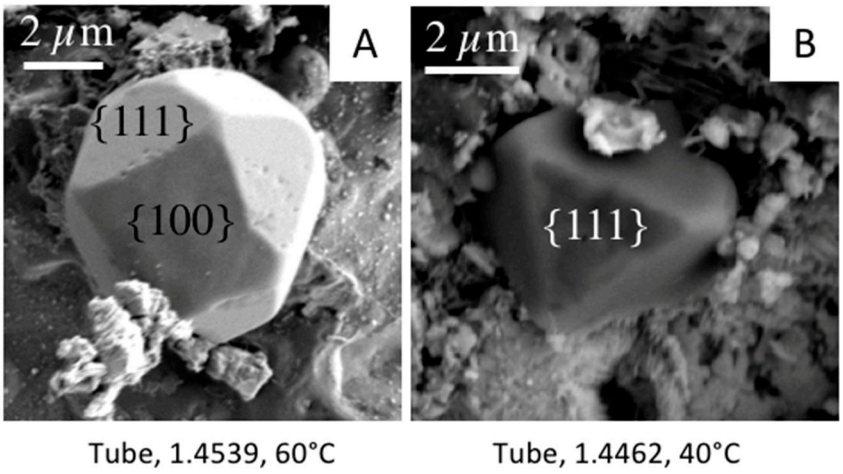

Figure 17. PbS cuboctahedron (**A**) and PbS octahedron (**B**) with their indexed faces, observed in two tubes made of 1.4539, at 60 °C (**A**) and 1.4462, at 40 °C (**B**).

Thus, cubes and cubic-derived shapes were observed on three different alloys and at temperatures from 65 to 40 °C (Table 4).

5. Fibro-Radiated Botryoidal Shape

The fibro-radiated botryoidal type (Figure 18A) is made of needles organized in 3D fan shape (Figure 18B,C) with several superimposed layers (Figure 18B,C). No to minor porosity is observed as opposed to coral shape. These three examples were observed occurred at a 50 °C temperature, on three different alloys. Table 2 shows all the locations where botryoids were observed, from 65 °C to 40 °C.

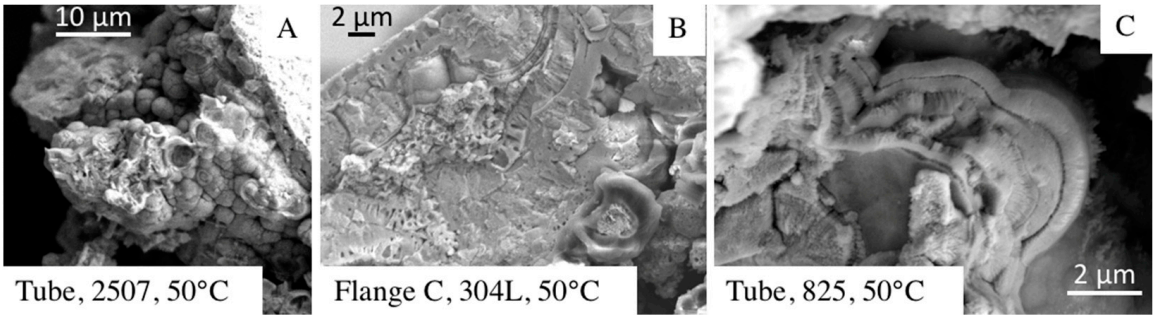

Figure 18. Fibro-radiated botryoidal shape from three different samples collected on a flange, and in two tubes of different alloys. All of the examples presented here were observed for a 50 °C temperature, but they also occurred at 65 °C and 40 °C (see Table 2). (**A**) general view, on a tube made of 2507 at 50 °C, (**B**,**C**) close view of a cross-section of botryoid on a flange and on a tube, at 50 °C.

Table 2 recapitulates all of the shapes that were observed by SEM, as a function of the location inside the SHEx, the alloy type and the temperature. Some samples do not show any characteristic crystal shapes, because of their poor quality (tubes of 1.4462 and 3.7035 alloys, Table 4). In the other samples, the coral shape is the most widely observed, whatever the alloy and the temperature. Other crystal shapes are frequently found in association with it in samples collected in tubes. Cubes are associated with coral shape in the west water box and on a flange, and in association with needles in both water boxes and in some tubes. Dendrites were observed in great abundance and not in association with other shapes in the industrial installation and in the entrance. The only dendrite found on a flange appears to be free on the surface of the scale and not embedded in the deposit. The various shapes were observed whatever the temperature and the alloy, except for dendrites which were observed only at the highest temperature.

5. Discussion

Galena is studied in ore deposits for scientific and economical purposes [38–40], and because of its toxicity in mining environments [41–43]. Galena is also well known in the industry, in particular for its semi-conductor properties and is thus thoroughly studied [44–46]. Natural galena is rarely a pure PbS component and frequently contains arsenic [47] and antimony [40,48]. Various galena shapes and chemical compositions are reported in natural environments [49]. Laboratory growth experiments show that the shape and chemistry of galena crystals can be controlled by several factors among which time, temperature and concentration of elements in the solvent [44–46,50]. All these previous studies might be useful for understanding the growth process in the SHEx at Soultz, even though the chemistry of the solution and other parameters are different. As regards shapes of PbS crystals, the literature reports laboratory growth of hopper (skeletal) crystals [51], dendrites, nanocubes, and truncated nanocubes [50], dendrites with different shapes [52], nanocoral [53], and many others.

5.1. Structure and Chemistry of Scales

In the SHEx, scales occur either as a powder or as layered deposits (Table 4).

Table 4. Structure of the scales sampled in the SHEx.

Structure	Location	Flow
Powder	Industrial Entrance Exit	Turbulent
Layers	Water boxes Tubes Flange	Laminar Perpendicular

Where the flow is turbulent, the scales deposit as a powder. Layered deposits are structured into sub-layers likely related to the operation of the power plant. In tubes made of 1.4462, the scales occurred as two major layers which were difficult to extract together and fell into small pieces during sampling, inducing a poor quality of samples. Scales deposited in 3.7035 tubes were strongly attached to the metal and were difficult to collect, resulting also in a bad quality of samples. This explains the lack of information about crystal shapes for those two alloys (Table 2). The micro-porosity observed in the superimposed thin layers, as well as between and inside the crystals (coral-shape for example) might be due to local turbulence of the flow.

The deposits that formed in the SHEx indeed contain galena, whatever the occurrence (entrance, water boxes or exit), as indicated by XRD diagrams (Figure 7) when compared to [50] who also used Cobalt anticathod. Their characteristics are summarized in Table 5.

Table 5. Characteristics of galena crystals determined from XRD.

Sharp Peaks	Location of Peaks	Preferential Growth
Well-crystallized [52]	Face-centered cubic structure, Fm3 m space group [50] Based on JCPDS, 5-592 [51] or ASTM file card No. 030660020 [53]	Strong intensity of (200) reflection peak [50,51], thus, preferential growth in the <100> direction

XRD analyses of the scales indeed show the presence of galena but give no information about its chemistry which was surveyed by SEM-EDS. It is homogeneous with the systematic presence of As and Sb in varying abundance, in addition to Pb and S, which is a well-known phenomenon in natural ore systems [40,47,48]. The chemistry of scale surveyed by SEM-EDS is summarized in Table 6.

Table 6. Summary of the chemistry of scales as surveyed by SEM-EDS.

Location	Elements	Phases	Shapes
All samples	Pb, As, Sb, S	Galena As, Sb sulfosalts (e.g., dufrénoysite, Figure 7)	Various (Table 2) Undetermined
All samples	Na, Cl	Halite	Cubes (Figures 8, 11 and 14)

Other sulfosalts might also occur given the high relative amount of As and Sb given by EDS analyses, but their small abundance did not allow us to see them on the diffractograms. In addition, the semi-quantification performed thanks to SEM-EDS did not allow to determine either their presence or their amount in the samples.

Halite was detected by XRD neither in the SHEx entrance, nor in its exit, probably because of its too small abundance, but it was seen by SEM-EDS. Indeed, the intensity of the peaks related to halite in the water boxes is weak on the XRD patterns (Figure 7).

To summarize, the composition of scales is homogeneous whatever the metal on which they formed and whatever the temperature of deposition (from 65 °C to 40 °C). Thus, it appears that these two parameters (alloy and temperature) do not influence the chemistry of scales.

5.2. Thickness of Scales

It is to be noted that the measurement of the deposit thickness (Table 2) might be considered as only semi-quantitative. Indeed, it could not always be performed strictly perpendicular to the deposit, which induced an uncertainty in the obtained value. However, a general tendency is observed: the thickness increases (e.g., from 50 to 220 µm for 1.4410 tubes) when the temperature decreases (from 60 °C to 40 °C). The deposition of scales in an exchanger has several effects, some of them positive, such as protection against corrosion, others negative, such as insulation reducing the heat exchange and hence energy production, or the decrease of the diameter of tubes which reduces the fluid flow. The thicker the deposit, the better the protection against corrosion but the lower the energy production. The thickness of scales has thus to be carefully monitored and controlled by addition of inhibitors to the process and maintenance when necessary, in order to allow optimal energy production.

5.3. Conditions of Scale Formation

It is likely that halite crystals developed when the SHEx was dismantled, during its draining and drying, as they are not embedded in the scales and sometimes grew on the MS of the scales (Figure 8A).

The conditions for scale formation during the geothermal process are summarized in Table 7 which shows the changes undergone by the deposit through time, with a decreasing influence of metal.

Table 7. Summary of conditions for scale formation.

Order of Layer Formation	Layer Structure	Location	Influence of Metal
1st	Smooth (Figures 8D, 9A and 10)	Contact with metal	Strong
2nd	Smooth to rough (Figures 9 and 10)	Contact with 1st layer	Low to none
3rd	Smooth to rough	Contact with 2nd layer	Low to none
4th and more	Rough (Figures 8A,B and 10)	Contact with previous layer	None

The influence of alloy nature on the shape of galena crystals being eliminated, the likely influencing parameters that remain to explain the crystal shapes are the chemical composition of the brine, its temperature and the flow regime.

Dendrites were observed exclusively at the exit of the industrial installation and in the entrance of the SHEx. Indeed, dendrites are known to crystallize quickly [31], which is permitted by the highest temperature (75–65 °C) and the turbulence in these locations.

Abundant recent literature presents the conditions of galena synthesis in laboratory and the shapes of crystals obtained [44,45,51–56]. Shapes identical to those found in the SHEx are encountered in conditions described as hydrothermal, meaning with water as a solvent and maintained at a temperature of, for example, 80 °C [50] to 200 °C [45], with durations of 2 h [45] to 48 h [50]. Song et al. (2012) [44] report that the concentration of the solution and reaction time (24 h at 170 °C) are key parameters for obtaining controlled PbS crystal shapes. In those conditions, they report cubes, dendrites, stars, and wires. These various shapes are required for specific industrial uses where the optical, magnetic and electronic properties of semi-conductors are of high importance [45]. Other authors [52] conducted solvothermal syntheses meaning with organic solvents and imposed temperature conditions leading to PbS dendrites. Nanocoral shape was obtained by [53], by vapor-solid deposition at high temperature (1050 °C) and thus at conditions drastically different from ours. [51] provide examples of various shapes obtained at a constant temperature (120 °C) but for various synthesis durations (3 to 24 h). [57] report various shapes of PbS nanoparticles (cubic, needle-like, spherical) due to the use of a number of capping agents. Wang et al. (2003) [52] who conducted their syntheses at the constant 120 °C temperature with various starting agents and several solvents, including water, obtained various types of PbS dendrites and other shapes. Hence, all these experiments show that there is no clear relationship between the parameters of the synthesis and the shapes obtained.

At Soultz, the solvent of the brine is water, but the inhibitors that are injected in the process are composed of organic molecules which play a role in the crystallization of galena. In fact, when no such agent is used, mostly sulfates (barite group (Ba,Sr,Ca)SO_4 solid-solution) are produced in the URG [12] and at Soultz in particular [27,31,33].

In the case of galena crystallization (use of inhibitors), when it occurs as cubes or derived shapes it results from a preferential growth along <111> direction inducing {100} faces to develop, which is not consistent with the major growth in <100> direction deduced from XRD. However, this is not abnormal since cubes and cubic-derived shapes are rarely found. Indeed, [54] proposed relations between crystal structure and crystal morphology on an energy basis. According to [54] the morphology of a crystal is governed by chains of strong bonds running through the structure, called periodic bond chain (P.B.C.) vectors. Crystal faces are divided into three classes. Flat faces (F) contain two or more coplanar P.B.C. vectors and are the most important faces. Stepped faces (S) are parallel to only one P.B.C vector and are of medium importance. Kinked (K) faces are parallel to no P.B.C. vector and are very rare or do not occur at all. For PbS crystals that belong to the fcc structure, F faces are {100}, S faces are {110} and K faces are {111}. According to Hartmann's and Perdok's theory [54] only F faces should appear at equilibrium, giving cubes as in Figure 16. In fact, during crystal growth, impurities such as the inhibitors used in the geothermal industrial process at Soultz, or As and Sb ions present in the geothermal brine, are adsorbed on K faces ({111} in this case) which promotes their development, together with that of cube (faces {100}), inducing the formation of cuboctahedrons (Figure 17A). In other cases (Figure 17B), only faces {111} develop, leading to octahedral crystals. Crystals with such planar faces (cubes, cuboctahedron, octahedron) appear in conditions of small growth rate, here in laminar flow, as opposed to dendrites which are obtained by a high growth rate in a single direction, here in the hottest and most turbulent flow. As seen in Figure 19, when a crystal grows, the faces which are kept at the end are those where the setting up of atoms is the slowest (faces {100} in the case of galena cubes). Indeed [55] indicates that the faster the growth in a given direction, the smaller the area of the face developed perpendicular to that direction (Figure 19, face {111}).

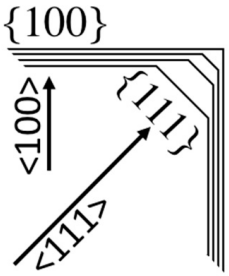

Figure 19. Schematic growth of a crystal face {xxx} as a function of the atom setting up rate in the direction perpendicular to that face <xxx>.

Hence, F faces are visible in the final crystal. Changes in morphology are related to F faces showing a different (higher) growth rate. As a consequence, dendrites and needles that develop in a preferential direction grow very quickly (turbulence and/or high temperature) while cubes and derived shapes grow slowly, in laminar flow and at temperatures which can be low (down to 40 °C). In Figure 14C, needles developed in three perpendicular directions grow on a preexisting 30µm wide galena cube. This succession of shapes might be controlled by very local changes in the parameters of the surrounding medium.

Table 8 summarizes the occurrence of galena crystal shapes.

Table 8. Occurrence of galena crystal shapes as a function of their location, the temperature and the flow.

Crystal Shape		Abundance among Location Samples	Temperature (°C)	Flow
Dendrite	+	Industrial, Entrance(flange)	75–65	Turbulent
Needle	++	Water box, flange, tubes	65–40	Turbulent, laminar
Coral	+++	Water box, flange, tubes	65–40	Turbulent, laminar
Cube	+	Water box, flange, tubes	65–40	Turbulent, laminar
Fibro-radiated	++	Water box, flange, tubes	65–40	Turbulent, laminar

Thus, except for dendrites, the location and hence turbulence degree of the place, nature of alloy and temperature are not controlling the shape of PbS crystals that formed in the SHEx, which can be found mixed at given places (Table 2) as opposed to what is described in the literature for syntheses in the laboratory. This might be due to the fact that in the SHEx, the parameters are not controlled as in the laboratory, which allows various shapes to crystallize at the same place. In addition, the temperature range is low, from 65 °C to 40 °C and is probably not discriminating for promoting specific crystal shapes.

The presence of As sulfosalts such as dufrénoysite, and maybe others containing Sb as indicated by the EDS semi-quantitative analyses (Table 5), might also be responsible for some of the shapes that were encountered during this study. However, it was not possible to identify them during SEM-EDS survey.

6. Conclusions and Outlook

One way to improve the energy production of geothermal power plants in the URG is to decrease the reinjection temperature. This might induce several problems in the power plants including cooling of the rock reservoir, promotion of a chemical disequilibrium into it, and increase of scaling phenomenon as observed for the samples collected in the SHEx at Soultz. When inhibitors are used, those scales are mostly composed of lead sulfide (galena, PbS) together with minor sulfosalts The galena crystals collected at the interface between the metals from which the SHEx was made and the geothermal fluid, after three months of operation, show a homogeneous chemical composition including As and Sb, whatever the alloy on which the scales deposited and whatever the temperature (65 °C to

40 °C). Thus, there is no influence of the alloy on the scaling phenomenon, as opposed to what is observed for corrosion. Those galena crystals show several shapes that cannot be evidently connected to the alloy, the temperature or the large-scale flow regime, except for dendrites. Indeed, the alloy is insulated from the fluid by the very first layers of deposit, the temperature does not vary drastically from the entrance to the exit of the SHEx (25 °C gradient only, at rather low temperatures), the chemical composition of the brine is constant during the industrial process (Ravier, personal communication), and after three months of operation, the scales are rough at the contact with the fluid and the flow is certainly very slow because of this rugosity, allowing the slow growth of crystals with various shapes including cubes and derived shapes. Dendrites are the only shape to be found exclusively at the highest temperature (65–75 °C) and in a turbulent environment. To go further, investigation could be performed with Raman to characterize the sulfosalts likely present in the samples, and with XANES to assess the oxidation state of As, Pb and Sb. In addition, statistics of the various shapes encountered at the different locations ought to be performed to pinpoint likely influencing parameters at the micro-scale. Furthermore, one could also conduct laboratory experiments with the brine produced from the geothermal reservoir, and with varying parameters such as temperature, alloy, speed of flow rate, type and amounts of inhibitors, etc. Finally, at present, scales produced at Soultz have to be disposed of as waste due to their toxicity. One can rather imagine an industrial valorization, especially for those deposited at the entrance and exit of the exchangers where mostly dendrites are formed, which is a sought-after shape for the industry [52].

Author Contributions: Conceptualization, B.A.L. and M.L.; methodology, G.R., O.S., B.A.L., É.D., A.G., X.S.; validation, J.M., C.B., É.D., A.G., Ayming and H2020 MEET partners; formal analysis, B.A.L.; investigation, B.A.L.; resources, G.R., O.S., J.M., C.B., É.D.; data curation, B.A.L. and M.L.; writing—original draft preparation, B.A.L. and M.L.; writing—review and editing, R.L.H., J.M., C.B., G.R., O.S., É.D., G.T., X.S., A.G.; supervision, B.A.L., A.G., G.T; project administration, A.G., É.D., G.T.; funding acquisition, all the co-authors and H2020 MEET consortium. All authors have read and agreed to the published version of the manuscript. Authorship is limited to those who have contributed substantially to the work reported.

Funding: This project has received funding from the European Union's Horizon 2020 research and innovation program under grant agreement No 792037 (MEET project).

Acknowledgments: The authors thank the Soultz-Sous-Forêts site owner, GEIE Exploitation Minière de la Chaleur, for giving access to their geothermal installation. Valérie Granger (Orano) is acknowledged for XRD analysis and its interpretation. We gratefully thank Jean Hérisson (Ayming) for reviewing this paper as well as relationship with European Commission and overview of the H2020 MEET project. We gratefully acknowledge the two reviewers for their helpful review which greatly helped us to improve the manuscript.

Conflicts of Interest: The authors declare no conflict of interest. The funders had no role in the design of the study; in the collection, analyses, or interpretation of data; in the writing of the manuscript, or in the decision to publish the results.

References

1. Assad, M.E.H.; Bani-Hani, E.; Khalil, M. Performance of Geothermal Power Plants (Single, Dual, and Binary) to Compensate for LHC-CERN Power Consumption: Comparative Study. *Geotherm. Energy* **2017**, *5*, 17. [CrossRef]
2. Spinthaki, A.; Kamaratou, M.; Skordalou, G.; Petratos, G.; Tramaux, A.; David, G.; Demadis, K.D. A Universal Scale Inhibitor: A Dual Inhibition/Dispersion Performance Evaluation under Difficult Brine Stresses. *Geothermics* **2021**, *89*, 101972. [CrossRef]
3. van der Zwaan, B.; Dalla Longa, F. Integrated Assessment Projections for Global Geothermal Energy Use. *Geothermics* **2019**, *82*, 203–211. [CrossRef]
4. Shannon, D.W. Economic Impact of Corrosion and Scaling Problems in Geothermal Energy Systems. Master's Thesis, Battelle Pacific Northwest Labs, Richland, WA, USA, 1975.
5. Tardiff, G.E. Using Salton Sea Geothermal Brines for Electrical Power: A Review of Progress in Chemistry and Materials Technology, 1976 Status. In Proceedings of the Twelfth Intersociety Energy Conversion Engineering Conference, Washington, DC, USA, 28 August–2 September 1977.

6. Criaud, A.; Fouillac, C. Sulfide Scaling in Low Enthalpy Geothermal Environments: A Survey. *Geothermics* **1989**, *18*, 73–81. [CrossRef]
7. Scheiber, J.; Nitschke, F.; Seibt, A.; Genter, A. Geochemical and Mineralogical Monitoring of the Geothermal Power Plant in Soultz-Sous-Forêts (France). In Proceedings of the 37th Workshop on Geothermal Reservoir Engineering, Stanford, CA, USA, 30 January–1 February 2012; pp. 1033–1042.
8. Ngothai, Y.; Yanagisawa, N.; Pring, A.; Rose, P.; O'Neill, B.; Brugger, J. Mineral Scaling in Geothermal Fields: A Review. In Proceedings of the 2010 Australian Geothermal Energy Conference, Adelaide, Autralia, 17–19 November 2010; pp. 405–409.
9. Skinner, B.J.; White, D.E.; Rose, H.J.; Mays, R.E. Sulfides Associated with the Salton Sea Geothermal Brine. *Econ. Geol.* **1967**, *62*, 316–330. [CrossRef]
10. Sanjuan, B.; Millot, R.; Innocent, C.; Dezayes, C.; Scheiber, J.; Brach, M. Major Geochemical Characteristics of Geothermal Brines from the Upper Rhine Graben Granitic Basement with Constraints on Temperature and Circulation. *Chem. Geol.* **2016**, *428*, 27–47. [CrossRef]
11. Baticci, F.; Genter, A.; Huttenloch, P.; Zorn, R. Corrosion and Scaling Detection in the Soultz EGS Power Plant, Upper Rhine Graben, France. In Proceedings of the World Geothermal Congress, WGC2010, Bali, Indonesia, 25–30 April 2010.
12. Haas-Nüesch, R.; Heberling, F.; Schild, D.; Rothe, J.; Dardenne, K.; Jähnichen, S.; Eiche, E.; Marquardt, C.; Metz, V.; Schäfer, T. Mineralogical Characterization of Scalings Formed in Geothermal Sites in the Upper Rhine Graben before and after the Application of Sulfate Inhibitors. *Geothermics* **2018**, *71*, 264–273. [CrossRef]
13. Mouchot, J.; Genter, A.; Cuenot, N.; Scheiber, J.; Seibel, O.; Bosia, C.; Ravier, G. First Year of Operation from EGS Geothermal Plants in Alsace, France: Scaling Issues. In Proceedings of the 43rd Workshop on Geothermal Reservoir Engeneering, Stanford, CA, USA, 12–14 February 2018.
14. Dalmais, E.; Genter, A.; Trullenque, G.; Leoutre, E.; Leiss, B.; Wagner, B.; Mintsa, A.C.; Bär, K.; Rajsl, I. MEET Project: Toward the Spreading of EGS across Europe. In Proceedings of the European Geothermal Congress, Den Haag, The Netherlands, 11–14 June 2019.
15. Trullenque, G.; Genter, A.; Leiss, B.; Wagner, B.; Bouchet, R.; Léoutre, E.; Malnar, B.; Bär, K.; Rajšl, I. Upscaling of EGS in Different Geological Conditions: A European Perspective. In Proceedings of the 43rd Workshop on Geothermal Reservoir Engineering, Stanford, CA, USA, 12–14 February 2018.
16. Ravier, G.; Seibel, O.; Pratiwi, A.S.; Mouchot, J.; Genter, A.; Ragnarsdóttir, K.R.; Sengelen, X. Towards an Optimized Operation of the EGS Soultz-Sous-Forêts Power Plant (Upper Rhine Graben, France). In Proceedings of the European Geothermal Congress, Den Haag, The Netherlands, 11–14 June 2019.
17. Ledésert, B.A.; Hébert, R.L. How Can Deep Geothermal Projects Provide Information on the Temperature Distribution in the Upper Rhine Graben? The Example of the Soultz-Sous-Forêts-Enhanced Geothermal System. *Geosciences* **2020**, *10*, 459. [CrossRef]
18. Cuenot, N.; Charléty, J.; Dorbath, L.; Haessler, H. Faulting Mechanisms and Stress Regime at the European HDR Site of Soultz-Sous-Forêts, France. *Geothermics* **2006**, *35*, 561–575. [CrossRef]
19. Gunnarsson, I.; Arnórsson, S. Impact of Silica Scaling on the Efficiency of Heat Extraction from High-Temperature Geothermal Fluids. *Geothermics* **2005**, *34*, 320–329. [CrossRef]
20. Haklıdır, F.S.T.; Balaban, T.Ö. A Review of Mineral Precipitation and Effective Scale Inhibition Methods at Geothermal Power Plants in West Anatolia (Turkey). *Geothermics* **2019**, *80*, 103–118. [CrossRef]
21. Hardardóttir, V.; Ármannsson, H.; Þórhallsson, S. Characterization of Sulfide-Rich Scales in Brine at Reykjanes. In Proceedings of the World Geothermal Congress 2005, Antalya, Turkey, 24–29 April 2005.
22. Jamero, J.; Zarrouk, S.J.; Mroczek, E. Mineral Scaling in Two-Phase Geothermal Pipelines: Two Case Studies. *Geothermics* **2018**, *72*, 1–14. [CrossRef]
23. Köhl, B.; Grundy, J.; Baumann, T. Rippled Scales in a Geothermal Facility in the Bavarian Molasse Basin: A Key to Understand the Calcite Scaling Process. *Geotherm. Energy* **2020**, *8*, 1–27. [CrossRef]
24. Kristmannsdóttir, H. Types of Scaling Occurring by Geothermal Utilization in Iceland. *Geothermics* **1989**, *18*, 183–190. [CrossRef]
25. Mundhenk, N. Corrosion and Scaling in Utilization of Geothermal Energy in the Upper Rhine Graben. Ph.D. Thesis, Karlsruher Instituts für Technologie (KIT), Karlsruhe, Germany, 2013. [CrossRef]
26. Nitschke, F.; Scheiber, J.; Kramar, U.; Neumann, T. Formation of Alternating Layered Ba-Sr-Sulfate and Pb-Sulfide Scaling in the Geothermal Plant of Soultz-Sous-Forêts. *Neues Jahrb. Für Mineral. Abh. J. Mineral. Geochem.* **2014**, *191*, 145–156. [CrossRef]
27. Raymond, J.; Williams-Jones, A.E.; Clark, J.R. Mineralization Associated with Scale and Altered Rock and Pipe Fragments from the Berlin Geothermal Field, El Salvador; Implications for Metal Transport in Natural Systems. *J. Volcanol. Geotherm. Res.* **2005**, *145*, 81–96. [CrossRef]
28. Reyes, A.G.; Trompetter, W.J.; Britten, K.; Searle, J. Mineral Deposits in the Rotokawa Geothermal Pipelines, New Zealand. *J. Volcanol. Geotherm. Res.* **2003**, *119*, 215–239. [CrossRef]
29. Genter, A.; Cuenot, N.; Melchert, B.; Moeckes, W.; Ravier, G.; Sanjuan, B.; Sanjuan, R.; Scheiber, J.; Schill, E.; Schmittbuhl, J. Main achievements from the multi-well EGS Soultz project during geothermal exploitation from 2010 and 2012. In Proceedings of the European Geothermal Congress, Pisa, Italy, 3–7 June 2013.
30. Scheiber, J.; Seibt, A.; Birner, J.; Genter, A.; Cuenot, N.; Moeckes, W. Scale Inhibition at the Soultz-Sous-Forêts (France) EGS Site: Laboratory and on-Site Studies. In Proceedings of the World Geothermal Congress 2015, Melbourne, Australia, 16–24 April 2015.

31. Sanjuan, B.; Millot, R.; Dezayes, C.; Brach, M. Main Characteristics of the Deep Geothermal Brine (5 Km) at Soultz-Sous-Forêts (France) Determined Using Geochemical and Tracer Test Data. *Comptes Rendus Geosci.* **2010**, *342*, 546–559. [CrossRef]
32. Cuenot, N.; Goerke, X.; Guery, B.; Bruzac, S.; Sontot, O.; Meneust, P.; Maquet, J.; Vidal, J. Evolution of the Natural Radioactivity within the Soultz Geothermal Installation. In Proceedings of the Soultz Geothermal Conference 2011, Soultz-Sous-Forêts, France, 5–6 October 2011; Volume 5, p. 19.
33. Mouchot, J.; Scheiber, J.; Florencio, J.; Seibt, A.; Jähnichen, S. Scale and Corrosion Control Program, Example of Two Geothermal Plants in Operation in the Upper Rhine Graben. In Proceedings of the European Geothermal Congress 2019, Den Haag, The Netherlands, 11–14 June 2019.
34. He, S.; Oddo, J.E.; Tomson, M.B. The Inhibition of Gypsum and Barite Nucleation in NaCl Brines at Temperatures from 25 to 90 °C. *Appl. Geochem.* **1994**, *9*, 561–567. [CrossRef]
35. Karlsdottir, S.N.; Ragnarsdottir, K.R.; Thorbjornsson, I.O.; Einarsson, A. Corrosion Testing in Superheated Geothermal Steam in Iceland. *Geothermics* **2015**, *53*, 281–290. [CrossRef]
36. Karlsdottir, S.N.; Thorbjornsson, I.O.; Ragnarsdottir, K.R.; Einarsson, A. Corrosion Testing of Heat Exchanger Tubes in Steam from the IDDP-1 Exploratory Geothermal Well in Krafla, Iceland. In Proceedings of the CORROSION 2014, San Antonio, TX, USA, 9–13 March 2014.
37. Ravier, G.; Huttenloch, P.; Scheiber, J.; Perrot, V.; Sioly, J.L. Design, Manufacturing and Commissioning of the ECOGI's Heat Exchangers at Rittershoffen (France): A Case Study. In Proceedings of the European Geothermal Conference, Strasbourg, France, 19–24 September 2016.
38. Apopei, A.I.; Damian, G.; Buzgar, N.; Buzatu, A. Mineralogy and Geochemistry of Pb–Sb/As-Sulfosalts from Coranda-Hondol Ore Deposit (Romania)—Conditions of Telluride Deposition. *Ore Geol. Rev.* **2016**, *72*, 857–873. [CrossRef]
39. Martínez-Abad, I.; Cepedal, A.; Arias, D.; Fuertes-Fuente, M. The Au–As (Ag–Pb–Zn–Cu–Sb) Vein-Disseminated Deposit of Arcos (Lugo, NW Spain): Mineral Paragenesis, Hydrothermal Alteration and Implications in Invisible Gold Deposition. *J. Geochem. Explor.* **2015**, *151*, 1–16. [CrossRef]
40. Pitcairn, I.K.; Olivo, G.R.; Teagle, D.A.; Craw, D. Sulfide Evolution during Prograde Metamorphism of the Otago and Alpine Schists, New Zealand. *Can. Mineral.* **2010**, *48*, 1267–1295. [CrossRef]
41. Medunić, G.; Bucković, D.; Crnić, A.P.; Bituh, T.; Srček, V.G.; Radošević, K.; Bajramovic, M.; Zgorelec, Z. Sulfur, Metal (Loid) s, Radioactivity, and Cytotoxicity in Abandoned Karstic Raša Coal-Mine Discharges (the North Adriatic Sea). *Rud. Geološko Naft. Zb.* **2020**, *35*. [CrossRef]
42. Majzlan, J.; Drahota, P.; Filippi, M. Parageneses and Crystal Chemistry of Arsenic Minerals. *Rev. Mineral. Geochem.* **2014**, *79*, 17–184. [CrossRef]
43. Karakaya, N.; Karakaya, M.C. Toxic Element Contamination in Waters from the Massive Sulfide Deposits and Wastes around Giresun, Turkey. *Turk. J. Earth Sci.* **2014**, *23*, 113–128. [CrossRef]
44. Song, C.; Jiang, L.; Zhang, Y.; Pang, L.; Wang, D. Shape Controllable Growth of PbS Polyhedral Crystals. *Cryst. Res. Technol.* **2012**, *47*, 1008–1013. [CrossRef]
45. Ding, B.; Shi, M.; Chen, F.; Zhou, R.; Deng, M.; Wang, M.; Chen, H. Shape-Controlled Syntheses of PbS Submicro-/Nano-Crystals via Hydrothermal Method. *J. Cryst. Growth* **2009**, *311*, 1533–1538. [CrossRef]
46. Ni, Y.; Wei, X.; Hong, J.; Ma, X. Hydrothermal Preparation of PbS Crystals and Shape Evolution. *Mater. Res. Bull.* **2007**, *42*, 17–26. [CrossRef]
47. Radosavljević-Mihajlović, A.S.; Stojanović, J.N.; Radosavljević, S.A.; Pačevski, A.M.; Vuković, N.S.; Tošović, R.D. Mineralogy and Genetic Features of the Cu-As-Ni-Sb-Pb Mineralization from the Mlakva Polymetallic Deposit (Serbia)—New Occurrence of (Ni-Sb)-Bearing Cu-Arsenides. *Ore Geol. Rev.* **2017**, *80*, 1245–1258. [CrossRef]
48. Adamczyk, Z.; Nowińska, K.; Melaniuk-Wolny, E.; Szewczenko, J. Variation of the Content of Accompanying Elements in Galena in Pyrometallurgical Process of Zinc and Lead Production. *Acta Montan. Slovaca* **2013**, *18*, 158–163.
49. Hagni, R.D. Platy Galena from the Viburnum Trend, Southeast Missouri: Character, Mine Distribution, Paragenetic Position, Trace Element Content, Nature of Twinning, and Conditions of Formation. *Minerals* **2018**, *8*, 93. [CrossRef]
50. Singh, K.; McLachlan, A.A.; Marangoni, D.G. Effect of Morphology and Concentration on Capping Ability of Surfactant in Shape Controlled Synthesis of PbS Nano-and Micro-Crystals. *Colloids Surf. A Physicochem. Eng. Asp.* **2009**, *345*, 82–87. [CrossRef]
51. Zhu, J.; Duan, W.; Sheng, Y. Uniform PbS Hopper (Skeletal) Crystals Grown by a Solution Approach. *J. Cryst. Growth* **2009**, *311*, 355–357. [CrossRef]
52. Wang, D.; Yu, D.; Shao, M.; Liu, X.; Yu, W.; Qian, Y. Dendritic Growth of PbS Crystals with Different Morphologies. *J. Cryst. Growth* **2003**, *257*, 384–389. [CrossRef]
53. Obaid, A.S.; Mahdi, M.A.; Hassan, Z. Nanocoral PbS Thin Film Growth by Solid-Vapor Deposition. *Optoelectron. Adv. Mater. Rapid Commun.* **2012**, *6*, 422–426.
54. Hartman, P.; Perdok, W.G. IUCr On the Relations between Structure and Morphology of Crystals. Available online: https://scripts.iucr.org/cgi-bin/paper?a01327 (accessed on 11 December 2020).
55. Pandey, G.; Shrivastav, S.; Sharma, H.K. Role of Solution PH and SDS on Shape Evolution of PbS Hexagonal Disk and Star/Flower Shaped Nanocrystals in Aqueous Media. *Phys. E Low Dimens. Syst. Nanostruct.* **2014**, *56*, 386–392. [CrossRef]

56. Esmaeili, E.; Sabet, M.; Salavati-Niasari, M.; Saberyan, K. Synthesis and Characterization of Lead Sulfide Nanostructures with Different Morphologies via Simple Hydrothermal Method. *High. Temp. Mater. Process.* **2016**, *35*, 559–566. [CrossRef]
57. Patel, A.A.; Wu, F.; Zhang, J.Z.; Torres-Martinez, C.L.; Mehra, R.K.; Yang, Y.; Risbud, S.H. Synthesis, Optical Spectroscopy and Ultrafast Electron Dynamics of PbS Nanoparticles with Different Surface Capping. *J. Phys. Chem. B* **2000**, *104*, 11598–11605. [CrossRef]